Unravelling the Role of Electron Acceptors for the Universal Enhancement of Charge Transport in Quinoid-Donor-Acceptor Polymers for High-Performance Transistors

Huanhuan Liang, Cheng Liu, Zesheng Zhang, Xuncheng Liu, Quanfeng Zhou, Guohui Zheng, Xiu Gong, Lan Xie, Chen Yang, Lianjie Zhang, Bo He, Junwu Chen* and Yi Liu**

H. Liang, C. Liu, Prof. X. Liu, Q. Zhou
College of Materials and Metallurgy
Guizhou University
Guiyang 550025, P. R. China
Email: xcliu3@gzu.edu.cn

Z. Zhang, Prof. L. Zhang, Prof. J. Chen
Institute of Polymer Optoelectronic Materials and Devices
State Key Laboratory of Luminescent Materials and Devices
South China University of Technology
Guangzhou 510640, P. R. China
Email: psjwchen@scut.edu.cn

Dr. G. Zheng, Dr. X. Gong
College of Physics
Guizhou University
Guiyang 550025, P. R. China

Prof. L. Xie
State Key Laboratory of Public Big Data
Guizhou University
Guiyang 550025, P. R. China

Prof. C. Yang
College of Big Data and Information Engineering
Guizhou University
Guiyang 550025, P. R. China

Dr. B. He, Dr. Y. Liu
The Molecular Foundry
Lawrence Berkeley National Laboratory
One Cyclotron Road, Berkeley, CA 94720, USA
Email: yliu@lbl.gov

Dr. B. He, Dr. Y. Liu
Materials Sciences Division
Lawrence Berkeley National Laboratory
One Cyclotron Road, Berkeley, CA 94720, USA

Keywords: charge transport, electron acceptors, morphology, organic field-effect transistors, quinoid-donor-acceptor strategy

Abstract: The quinoid-donor-acceptor (Q-D-A) strategy has recently emerged as a promising approach for constructing high mobility semiconducting polymers. In order to fully explore the potential of this strategy in improving the charge transport and elucidating the structure-property-performance relationships in Q-D-A polymers, a series of new polymers with different electron acceptor units and backbone coplanarity have been synthesized and characterized. All of the resulting Q-D-A polymers exhibit much more planar backbone conformations in comparison to their donor-acceptor (D-A) counterparts. Moreover, organic field-effect transistors (OFETs) based on Q-D-A polymers exhibit excellent effective hole mobilities in a range of 0.44 to 3.35 $cm^2 V^{-1} s^{-1}$, most of which are orders of magnitude higher than those of their corresponding D-A polymers. Notably, the hole mobility of 3.35 $cm^2 V^{-1} s^{-1}$ is among the highest for the quinoidal-aromatic polymers characterized by conventional spin-coating methods. Furthermore, the role of electron acceptors in Q-D-A polymers has been comprehensively investigated. Polymers with stronger acceptor units are more inclined to deliver edge-on lamellas, high film crystallinity, small effective hole masses and decent operational stability. The detailed structure-property-device performance relationship will pave the way towards high performance semiconducting polymers using the potent Q-D-A strategy.

1. Introduction

Organic field-effect transistors (OFETs) are gaining special interest as the primary component of complementary circuits for their potential use in flexible displays and other electronic devices.[1] Semiconducting polymers have received great attention during the past two decades owing to their promising utilization as the active layer for cost-effective manufacturing of large-area OFETs.[2] Storage stability under ambient conditions of semiconducting polymers employed in OFETs have improved a lot and approached to the sufficient level for practical usage.[3] Considering commercialization of OFETs, operational stability under bias is as critical as storage stability.[4] Therefore, pursuing high performing semiconducting polymers with efficient charge transport and sufficient operational stability has become a scientific goal.

The donor-acceptor (D-A) strategy has been used extensively for constructing semiconducting polymers with tailored optoelectronic properties,[5] where thiophene-containing units are the most widely used electron donors.[6] The combination of oligothiophenes and electron acceptors into the backbone has been a successful approach to endowing the resulting polymers with sufficient solubilities, high crystallinity, desired thin film morphology and high charge carrier transport mobility.[7] Polymer backbone coplanarity is another design consideration that plays a key role in determining conjugation length, intermolecular interactions, thin film crystallinity and chain orientation, which has a profound impact on the performance of OFET devices.[8] To further accelerate the carrier transport, backbone coplanarity of polymers based on oligothiophenes and acceptors need to be optimized. The commonly used strategies include: (1) insertion of vinylene spacers into the backbone;[9] (2) conformation locking via covalent/non covalent bonds;[10] and (3) incorporation of novel acceptor units with five-membered-ring-fused structure.[11] However, those methods generally suffer from limited improvement of whole backbone coplanarity and/or complicated synthetic route. Therefore, how to efficiently enforce the backbone coplanarity of semiconducting polymers based on oligothiophenes and acceptors by facile synthesis remains a fundamental issue.

Quinoidal-aromatic conjugated polymers, with intrinsic quinoidal structures, possess high coplanarity and rigidity of the polymer backbone because of minimization of bond length alternation (BLA), which show promising charge transport properties though still lagging behind D-A conjugated polymers.[12] Previously we have discovered a smallest stable quinoidal building block with a “charge-neutral” nature, *para*-azaquinodimethane (*p*-AQM), which was incorporated into conjugated backbone to tune the bandgap and realize high

crystallinity and carrier mobility,[13] and has also been implemented in diverse applications.[14] We recently proposed an unprecedented quinoid-donor-acceptor (Q-D-A) strategy by combining the quinoid, donor and acceptor units in the backbone to construct quinoidal-aromatic conjugated polymers with exceptional charge carrier transporting characteristics.[15] Inserting *p*-AQM into the backbone of D-A polymers based on terthiophene and benzothiadiazole (BT) unit could efficiently enforce the backbone coplanarity, leading to four orders of magnitude higher mobility than that of corresponding D-A polymers. This encouraging result opens the door to high mobility semiconductors by leveraging the full potential of the Q-D-A strategy, which motivates a more comprehensive study to inform rational molecular design for better performances.

Herein, we employed the Q-D-A strategy to synthesize a series of polymers with different acceptor units of varying strength (**Scheme 1**). Coplanar backbone conformation analyses using density functional theory (DFT) calculations suggested that all the Q-D-A polymer backbone coplanarity could be significantly reinforced compared with the twisted backbones of their D-A analogues. In addition, OFET devices based on Q-D-A polymers show orders-of-magnitude higher hole mobilities than those of their corresponding D-A polymers (Figure S1, Table S1, Supporting Information).[16] Thin film morphology studies by grazing-incidence wide-angle X-ray scattering (GIWAXS) and OFETs device stability evaluation reveal that film crystallinity, crystallite orientation and operational stability strongly correlate with the acceptor strength. This works provides a deep insight into the relationships of structure-property-performance in Q-D-A polymers, which will be essential to accelerate the development of high performance semiconducting polymers.

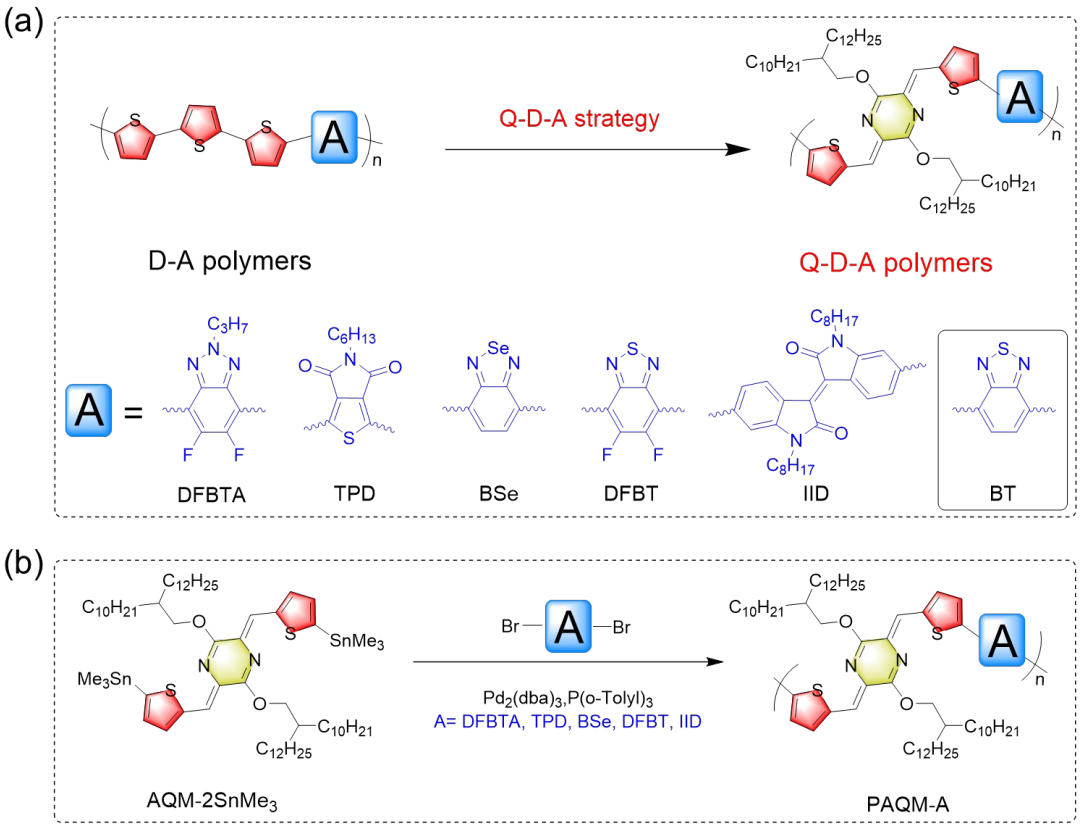

Scheme 1. a) Molecular structures of Q-D-A polymers reported in this work and general chemical structures of corresponding D-A polymers reported previously. b) Synthetic route to the five Q-D-A polymers.

2. Results and Discussion

2.1. Synthesis of the Polymers

All of the Q-D-A polymers were synthesized by Pd-catalyzed Stille copolymerization between the distannylated monomer AQM-2SnMe$_3$ and the corresponding dibromo monomers A-2Br at 135 °C for 3 days (**Scheme 1b**). The quinoid monomer AQM-2SnMe$_3$ was succinctly synthesized according to our previous work.[13b] Five commercially available dibromo monomers A-2Br were selected according to their gradually varied electron acceptor strength. The desired products were purified by successive Soxhlet extraction in air with methanol, acetone and ethyl acetate to remove low molecular weight fractions and catalyst residues, followed by reprecipitating the chloroform extracted fractions into methanol. The polymers are denoted as PAQM-DFBTA, PAQM-TPD, PAQM-BSe, PAQM-DFBT and PAQM-IID, in accordance with the use of 5,6-difluorobenzotriazole (DFBTA), thienopyrrole-4,6-dione (TPD), benzoselenadiazole (BSe), 5,6-difluorobenzothiadiazole (DFBT) and isoindigo (IID) as the acceptor units, respectively. All the polymers exhibit adequate solubilities in common solvents such as chloroform (CF), chlorobenzene (CB) and 1,2-

dichlorobenzene, resulting in good processability when used in OFET devices. High temperature size exclusion chromatography (SEC) was conducted at 150 °C with 1,2,4-trichlorobenzene as the eluent to determine the polymer molecular weight, as shown in **Table 1**. The number-average molecular weights (M_n) of the five polymers are in the range of 10.1-16.0 kDa and comparable to the previous reported PAQM-BT of 16.2 kDa. The small M_n variation ensures a comparable molecular weight of polymers for the systematic study of polymer properties and device performance. In addition, thermogravimetric analysis (TGA) and differential scanning calorimetry (DSC) analysis were performed to evaluate the thermal properties of the new Q-D-A polymers. As depicted in Figure S2 (Supporting Information), all polymers possess good thermal stability with a decomposition temperature (T_d) of 365–379 °C at a 5% weight loss. Furthermore, no obvious phase-transition peaks appeared in the heating or cooling cycles of DSC analysis within the temperature range of 30–300 °C, reflecting the backbone rigidity of the new Q-D-A polymers, which agree well with our previous work.[15]

2.2. Optical and Optoelectronic Properties

The UV-vis absorption spectra for five Q-D-A polymers were acquired from solutions in dilute chlorobenzene and spun-cast thin films prepared from chlorobenzene, as shown in **Figure 1**, **Table 1** and Figure S**3** (Supporting Information). The absorption spectra and other relevant data of PAQM-BT were also included for comparison. In dilute chlorobenzene, all the Q-D-A

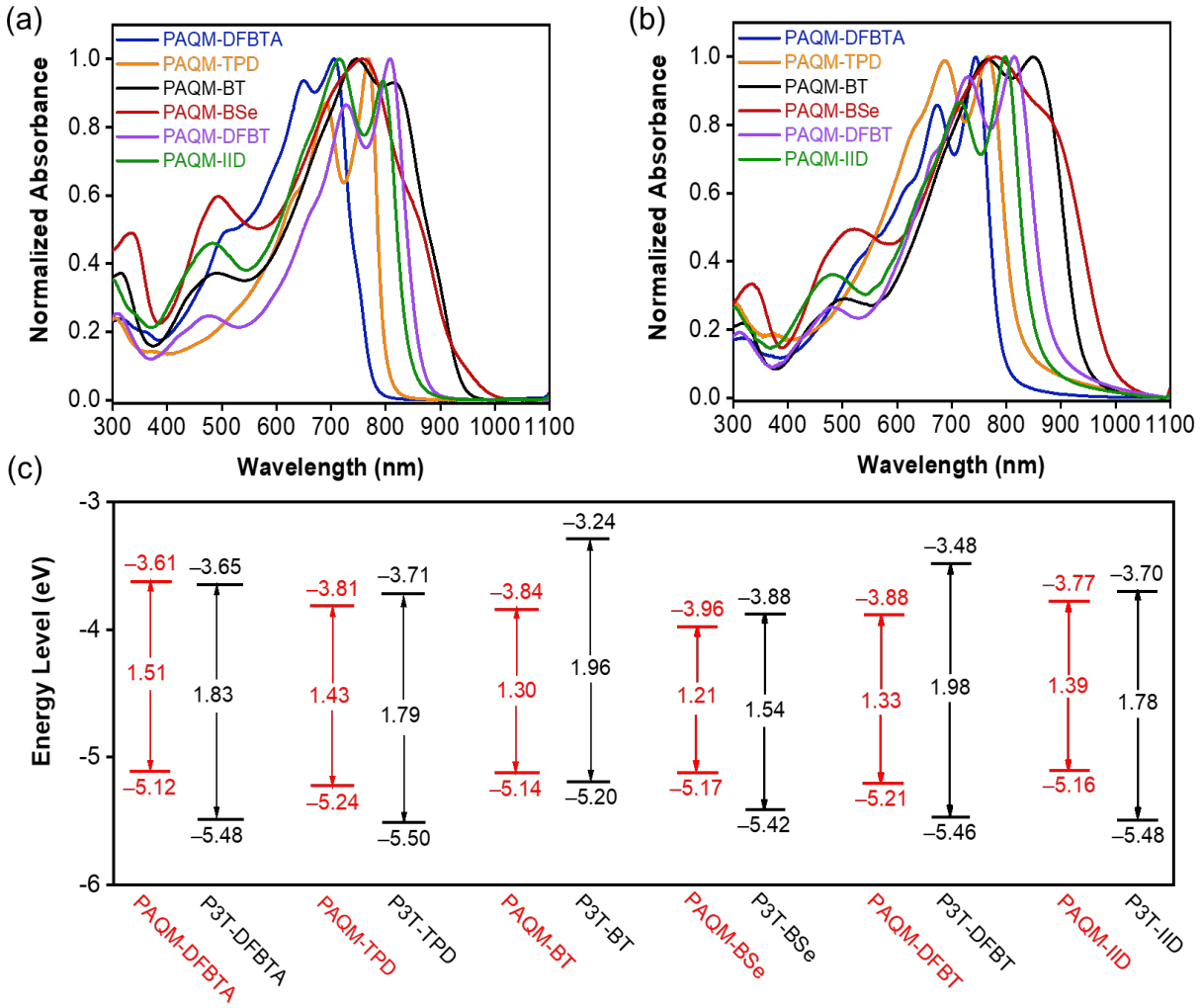

Figure 1. Normalized UV-vis absorption spectra of a) Q-D-A polymer solutions in chlorobenzene at room temperature and b) Q-D-A polymer thin films. c) Diagram of energy levels and bandgaps of Q-D-A polymers reported in this work and the corresponding D-A polymers from the literature.[16]

polymers exhibited pronounced double absorption peaks in the long wavelength region of 600-

900 nm, despite the relatively weak shoulder peak at 877 nm of PAQM-BSe, indicating strong interchain interactions and ordered pre-aggregated states in solutions.[17] However, their corresponding D-A polymers displayed obviously blue-shifted solution absorption and totally different shape with only single peak in the long wavelength region, except that P3T-TPD showed two additional inconspicuous shoulder peaks. The contrast suggested that the insertion of *p*-AQM decreased the bandgap and enhanced the interchain interaction of Q-D-A polymers. In addition, we conducted the temperature dependent absorption studies of all Q-D-

A polymers in chlorobenzene to evaluate the relative strength of interchain interaction (Figure S4, Supporting Information). When the solution was heated from 15 to 95 °C, the intensity of the longer wavelength shoulder decreased continuously and disappeared eventually for PAQM-IID and PAQM-BSe. PAQM-TPD and PAQM-BT displayed a slightly different behavior, with significant retention of their longer wavelength vibronic shoulders at 95°C. In contrast, the absorption of PAQM-DFBT and PAQM-DFBTA remained almost unchanged during the heating process with only a slight blue shift of the absorption. In most cases, higher temperature will favor more twisted backbone and decrease the conjugation length, mitigating the tendency to aggregate.[18] Considering that the longer wavelength shoulder is ascribed to interchain aggregation, it is apparent that the interchain interaction in PAQM-DFBT and PAQM-DFBTA is much stronger than other Q-D-A polymers, presumably due to the effect of fluorine atoms,[19] which are conducive for interchain charge hopping. When changing from solution to thin film (**Figure 1b**), the absorption behavior remained nearly unchanged with dual-band absorptions in longer wavelength and slightly red shifted by less than 50 nm, suggesting tight molecular packing in the film. Furthermore, the intensity of vibronic shoulder peak for all Q-D-A polymers showed modest but noticeable increase upon thermal annealing (Figure S5, Supporting Information), indicating the improvement in crystallinity and molecular ordering in annealed films,[8b] which is in good accordance with thin-film microstructure characterization (vide infra). The band gaps (E_g) estimated from the absorption edges are in the order of PAQM-DFBTA (1.51 eV)>PAQM-TPD (1.43 eV)>PAQM-IID (1.39 eV)>PAQM-DFBT (1.33 eV)>PAQM-BT (1.30 eV)>PAQM-BSe (1.21 eV). All the Q-D-A polymers showed significantly reduced bandgaps than those of their corresponding D-A polymers (**Figure 1c**).

Table 1. Summary of molecular weights, optical band gaps and electrochemical properties of the Q-D-A polymers.

Polymer	M_n[a)] [kDa]	PDI	Solution			Film			HOMO[c)] [eV]	LUMO[d)] [eV]
			λ_{max1} [nm]	λ_{max2} [nm]	E_g[b)] [eV]	λ_{max1} [nm]	λ_{max2} [nm]	E_g[b)] [eV]		
PAQM-DFBTA	16.0	1.90	651	706	1.56	674	744	1.51	–5.12	–3.61
PAQM-TPD	14.9	2.97	691	768	1.51	688	768	1.43	–5.24	–3.81
PAQM-BT[e)]	16.2	2.50	746	815	1.31	766	850	1.30	–5.14	–3.84
PAQM-BSe	10.1	1.65	491	877	1.27	781	882	1.21	–5.17	–3.96

PAQM-DFBT	14.3	2.28	728	808	1.40	729	814	1.33	–5.21	–3.88
PAQM-IID	12.2	2.12	716	795	1.43	714	798	1.39	–5.16	–3.77

[a)]Molecular weights estimated by high temperature SEC at 150 ℃. [b)]Optical bandgaps estimated on the basis of the absorption onset. [c)]Measured by cyclic voltammetry. [d)]Calculated by subtraction of film optical bandgap from HOMO level. [e)] Reported previously.

The frontier orbital energy levels of all present Q-D-A polymers were investigated using cyclic voltammetry (CV). As shown in **Figure 1c**, **Table 1** and Figure S6(Supporting Information), the highest occupied molecule orbital (HOMO) energy levels of these polymers are between –5.24 and –5.12 eV with a small variation, conforming that the HOMO level is mainly dependent on the electron donor units in Q-D-A polymers. In contrast, the lowest unoccupied molecular orbital (LUMO) energy levels of these polymers, estimated by subtracting the band gap values from the corresponding HOMO levels, lie in a wide range of –3.96 to –3.61 eV, suggesting that LUMO levels of Q-D-A polymers could be readily modified by selecting different electron acceptor unit. Comparing the energy levels of Q-D-A polymers and their previously reported corresponding D-A polymers (**Figure 1c**), it is apparent that the insertion of *p*-AQM unit could upshift HOMO levels and downshift LUMO levels simultaneously owing to the quinoidal characters of *p*-AQM moiety, with the exception of PAQM-DFBTA which has a slightly higher LUMO level than P3T-DFBTA.

2.3. Theoretical calculations

In order to illustrate the backbone geometry and explore the full potential of Q-D-A strategy in manipulating the backbone coplanarity, density functional theory (DFT) calculations were carried out using the B3LYP/ 6-311G (d,p) basis set with Gaussian 09 based on a trimer segment of each of the new Q-D-A polymers and their corresponding D-A polymers. For the sake of simplicity, the alkyl chains in all the segment were replaced by methyl groups. The optimized backbone geometries, dipole moments and frontier molecular orbital distributions are displayed in **Figure 2** and Figure S7 (Supporting Information), respectively. Large torsion angles of 10.4°–30.3° between the neighboring thiophene moieties, and of 0.0°–22.5° between the acceptor and thiophene moieties are present in the backbone of trimers of the D-A polymers, resulting in apparently twisted conformation. The nonplanarity reduces effective π-orbital overlap, decreases effective conjugation length and hinders π-π stacking interactions, all contributing to poorer charge transport. This low degree of backbone coplanarity correlates

well with their inferior hole mobilities, ranging from 1.68×10^{-3} to 5.85×10^{-1} cm^2 V^{-1} s^{-1} (Table S1,

Supporting Information).[16] In sharp contrast, by inserting *p*-AQM into the backbone of D-A polymers to substitute the central thiophene moiety, the dihedral angles between all neighboring moieties were dramatically decreased and the whole backbone coplanarity was greatly enforced. Furthermore, with the exception of PAQM-IID, the trimers of Q-D-A polymers were completely planar with all dihedral angles approaching 0°. In the case of PAQM-IID, despite that its backbone was not as planar as other Q-D-A polymers, which presumably was due to the

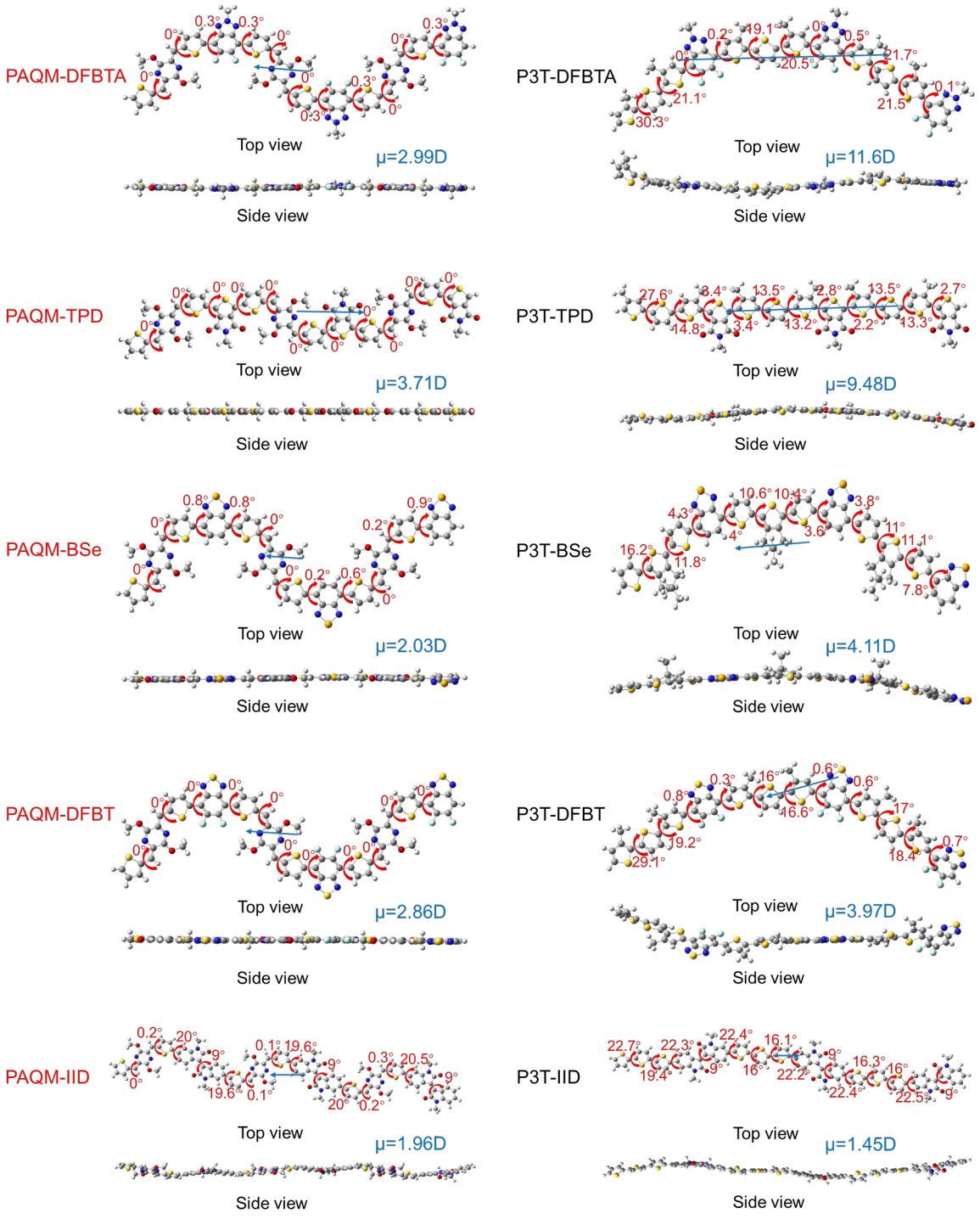

F

igure 2. Optimized geometries and net dipole moments of the trimeric segments of the Q-D-A polymers and the corresponding D-A polymers, in which alkyl chains are substituted with methyl groups to simplify the calculation.

larger size of its isoindigo core than other acceptor units, the dihedral angles between thiophene moieties and between thiophene and acceptor units decreased to ~0° and 20.5°,

respectively, which was smaller than that of its corresponding D-A polymer P3T-IID with slightly enforced backbone coplanarity.

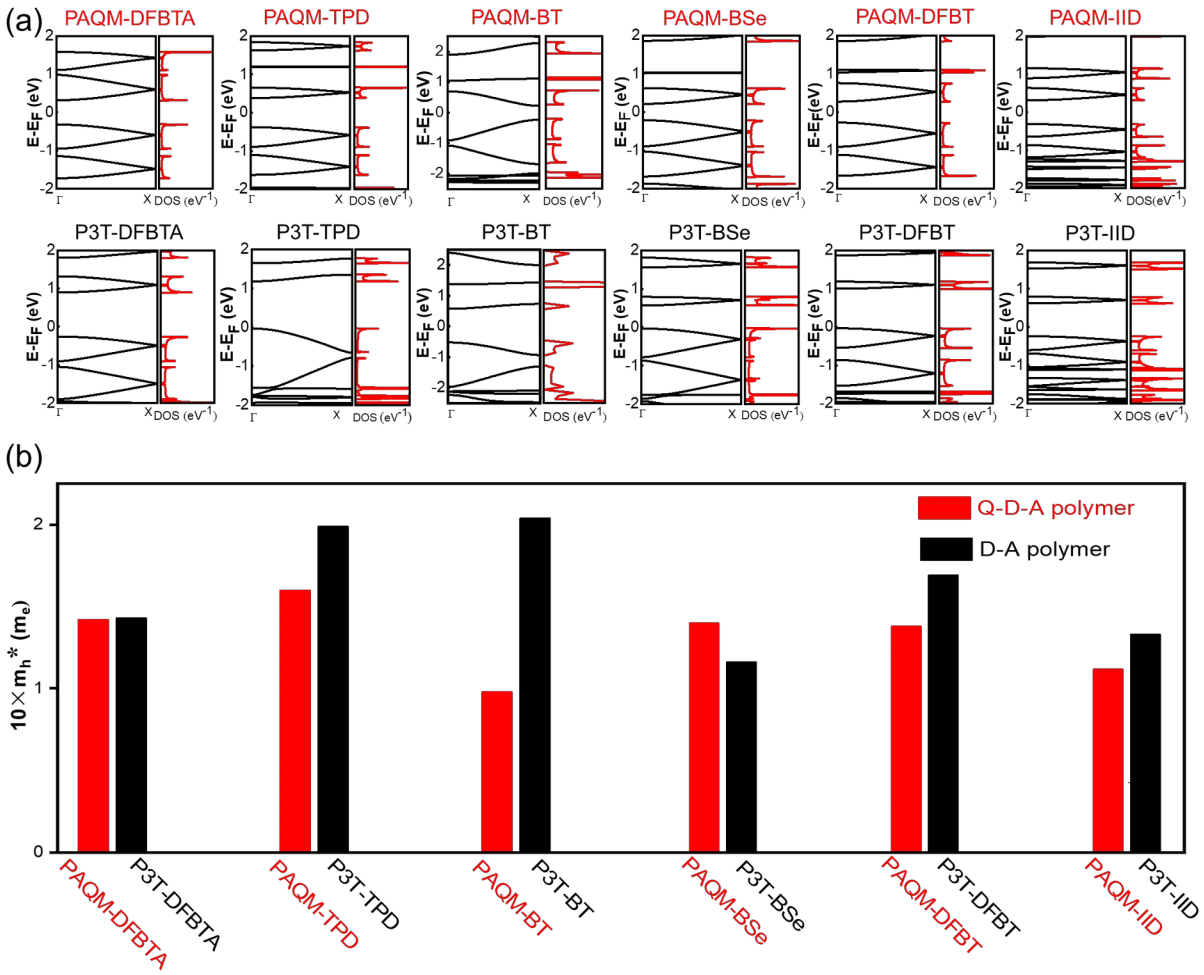

Figure 3. a) Band structures and partial densities of states (DOS) of the Q-D-A polymers and the corresponding D-A polymers calculated in this work. b) Comparison of effective hole masses of Q-D-A polymers and the corresponding D-A polymers.

Although the calculated energy levels are not identical to the experimental results, certain correlations between calculations and experimental results are found to be in good agreement with each other in this work (Figure S8, Supporting Information). Compared to D-A polymers, the predicted HOMO and LUMO levels of their corresponding Q-D-A polymers are upshifted and downshifted, respectively, while the trends are consistent with the experimental results, with the exception of PAQM-DFBTA which showed a comparable experimental LUMO level to that of P3T-DFBTA. In addition, the relative order of experimental HOMO levels for all six Q-D-A polymers correlates well with that of the calculated HOMO levels. For instances, PAQM-DFBTA exhibits the highest experimental

HOMO level among all the Q-D-A polymers, while DFT calculations also predicts its highest HOMO level. Moreover, the trend of change in calculated LUMO levels among Q-D-A polymers is in close agreement with the experimentally observed trend among Q-D-A polymers. The HOMO and LUMO levels were more spread out over the entire backbone of the trimers of Q-D-A polymers than those of D-A polymers, indicating faster intrachain charge transport along the Q-D-A polymer backbones. Polymers with enforced backbone coplanarity was expected to exhibit more efficient intrachain charge transport and interchain charge hopping due to the enhanced conjugation length and stronger interchain interactions derived from the highly planar conformations in comparison to their corresponding D-A polymers.[20] In order to verify that the intrachain charge transport along the Q-D-A polymer backbone is more efficient than that of its D-A analogue, theoretical calculations of effective hole masses (m_h*) for six Q-D-A polymers and six corresponding D-A polymers were carried out via the calculation of band structures and density of states using Vienna *ab initio* simulation package (VASP) with the Perdew-Burke-Ernzerhof (PBE) functional.[21] Band structures, partial densities of states (DOS) and calculated m_h* of Q-D-A and D-A polymers were shown in **Figure 3** and Figure S9 (Supporting Information), and summarized in **Table 2**. For comparison, relevant calculations of PAQM-BT are also included. A small m_h* indicates efficient charge transport along the backbone. With the exception of PAQM-BSe, the five Q-D-A polymers demonstrate smaller values of m_h* than that of their corresponding D-A polymers, evidencing that intrachain charge transport are more efficient in Q-D-A polymers, which would help increase carrier mobilities.

Table 2. OFET performances, reliability factor and effective hole masses of the Q-D-A polymers.

Polymer	$\mu_{h,claimed}$[a)] [$cm^2 V^{-1} s^{-1}$]	γ[b)] [%]	$\mu_{h,eff}$[c)] [$cm^2 V^{-1} s^{-1}$]	V_{th} [V]	$I_{on/off}$	S[d)] (V/dec)	$m_h^*(m_e)$[e)]
PAQM-DFBTA	0.71 (0.44 ± 0.12)	84.4	0.60	–16	10^3-10^4	–18	0.142
PAQM-TPD	0.72 (0.54 ± 0.09)	74.2	0.53	–25	10^2-10^3	–24	0.160
PAQM-BT[f)]	5.10 (4.35)[f)]	—[g)]	—[g)]	–13	10^3-10^4	—[g)]	0.098
PAQM-BSe	0.52 (0.25± 0.12)	84.8	0.44	–14	10^4-10^5	–12	0.140
PAQM-DFBT	4.11 (3.19 ± 0.63)	81.8	3.35	–17	10^3-10^4	–11	0.138
PAQM-IID	1.48 (1.02± 0.19)	73.5	1.08	–15	10^3-10^4	–15	0.112

[a)]Maximum mobility under optimized annealing conditions. Average mobilities were calculated based on 10 independent devices and listed in parentheses. [b)]Reliability factor γ calculated according to ref. [23]. [c)]Effective mobility obtained from the equation $\mu_{h,eff}$

$=\mu_{h,claimed}\times\gamma$. [d]Sub-threshold slope calculated according to ref. [25]. [e]Effective hole mass (m_h*) extracted from the theoretical calculations. m_e represents the mass of an electron. [f]Reported previously. [g]Not available.

2.4. OFET Fabrication and Characterization

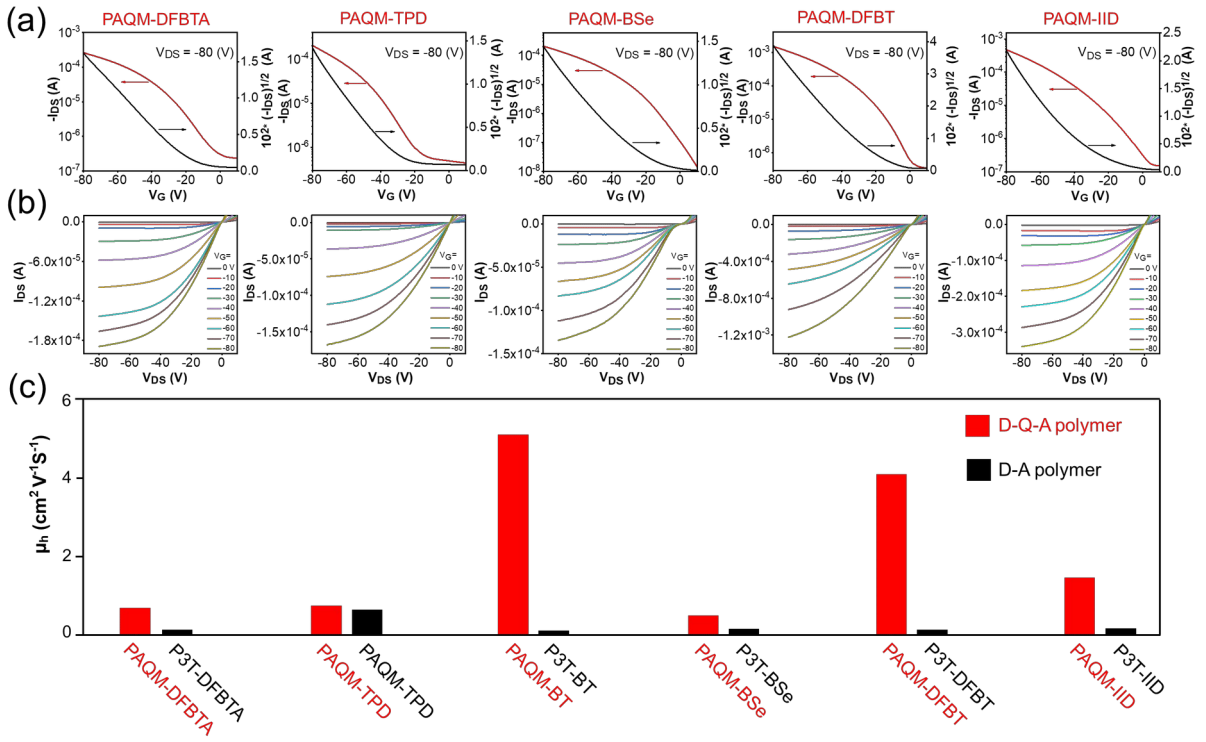

Figure 4. Typical a) transfer and b) output characteristics of OFETs based on Q-D-A polymers after thermal annealing at the optimized temperature. c) Comparison of maximum hole mobilities of Q-D-A polymers and the previously reported corresponding D-A polymers. [16]

In order to examine the charge transport properties of the present Q-D-A polymers, bottom-gate top-contact (BGTC) OFET devices were fabricated in an argon (Ar)-filled glovebox and measured in air. The semiconductor layers were formed by spin-coating 5 mg/mL CB/CF (mixture solvent, volume ratio=1:6) solutions onto a self-assembled monolayer (SAM) of *n*-octadecyltrichlorosilane (OTS)-modified SiO_2/heavily n-doped Si substrate and then annealed at the optimized temperature of 150 or 175 °C. Then ~40 nm thick gold (Au) was utilized as the source and drain electrodes. The fabrication details are provided in the Supporting Information. Characteristic transfer and output plots of transistors and device performances were shown and summarized in **Figure 4**, **Table 2,** Figure S10 and Table S2 (Supporting Information). For comparison, the relevant parameters of PAQM-BT

were also included. All the annealed Q-D-A polymers displayed excellent *p*-type transport properties with maximum hole mobility ($\mu_{h,\ claimed}$) in the range of 0.52 to 4.11 $cm^2\ V^{-1}\ s^{-1}$, which are higher than that of their corresponding D-A polymers,[16] correlating well with their enforced backbone coplanarity (**Figure 4**). Orders-of-magnitude higher hole mobilities could be achieved by modifying D-A polymers with Q-D-A strategy (Table S1, Supporting Information). Out of abundant precaution when evaluating high mobility OFETs to avoid overestimation,[22] we evaluated the reliability factor (γ) of our device results according to the previous literature.[23] As shown in **Table 2** and Figure S11 (Supporting Information), the γ values were estimated to be in the range of 73.5%-84.8%, which corresponded to the effective hole mobilities ($\mu_{h,\ eff}$) of 0.44 to 3.35 $cm^2\ V^{-1}\ s^{-1}$ for Q-D-A polymers-based OFETs. Specifically, devices based on PAQM-TPD, PAQM-BSe and PAQM-DFBTA showed moderate effective hole mobilities of approximately 0.50 $cm^2\ V^{-1}\ s^{-1}$, which were consistent with their relatively larger effective hole masses than those of PAQM-IID and PAQM-DFBT. As for PAQM-IID, its smallest effective hole mass of $0.112m_e$ correlated with a decent hole mobility of up to 1.08 $cm^2\ V^{-1}\ s^{-1}$. PAQM-DFBT displayed an impressive effective hole mobility of up to 3.35 $cm^2\ V^{-1}\ s^{-1}$, which was among the highest values for quinoidal-aromatic conjugated polymers characterized by conventional spin-coating deposition methods (Figure S12). In addition, Q-D-A polymers exhibited comparable on/off current ratio of ca. 10^4 except that PAQM-TPD showed a smaller and less desirable on/off current ratio of ca. 10^3. Low threshold voltage and low inverse sub-threshold slope are conducive to achieving maximum source-drain current at the minimum gate voltage, which are key factors for low-voltage operation.[24] However, a higher threshold voltage of –25 V and a higher inverse sub-threshold slope of 24 V dec^{-1} were calculated[25] for PAQM-TPD-based OFETs when compared to that of other Q-D-A polymers, which could be partially explained by its deepest HOMO level and the resulting injection barrier for holes from Au electrode and contact resistance.[26] The results demonstrate that the charge transport of Q-D-A polymers could be modulated by selecting different acceptor unit. When taking thermal annealing into consideration, all the OFET devices based on as-cast Q-D-A polymers displayed decent hole mobilities of 0.12–0.80 $cm^2\ V^{-1}\ s^{-1}$ (Figure S13, Supporting Information), consistent with the crystalline nature of as-cast films (vide infra). As shown in Table S2 (Supporting Information), thermal annealing led to remarkable improvement of hole mobilities for all the Q-D-A polymers, which correlated well with their enhanced crystallinity and pronouncedly interconnected domains of annealed films (vide infra).

2.5. Thin-Film Morphologies

To probe the crystalline nature and molecular orientation of Q-D-A polymers, GIWAXS measurements were performed. GIWAXS images and the relevant line-cut profiles of annealed Q-D-A polymer films are depicted in **Figure 5** and Figure S14 (Supporting Information). Thin films were annealed at 150 or 175 °C. For comparison, the relevant data of the PAQM-BT thin film annealed at 150 °C was also included. PAQM-DFBTA exhibited obvious (010) diffraction

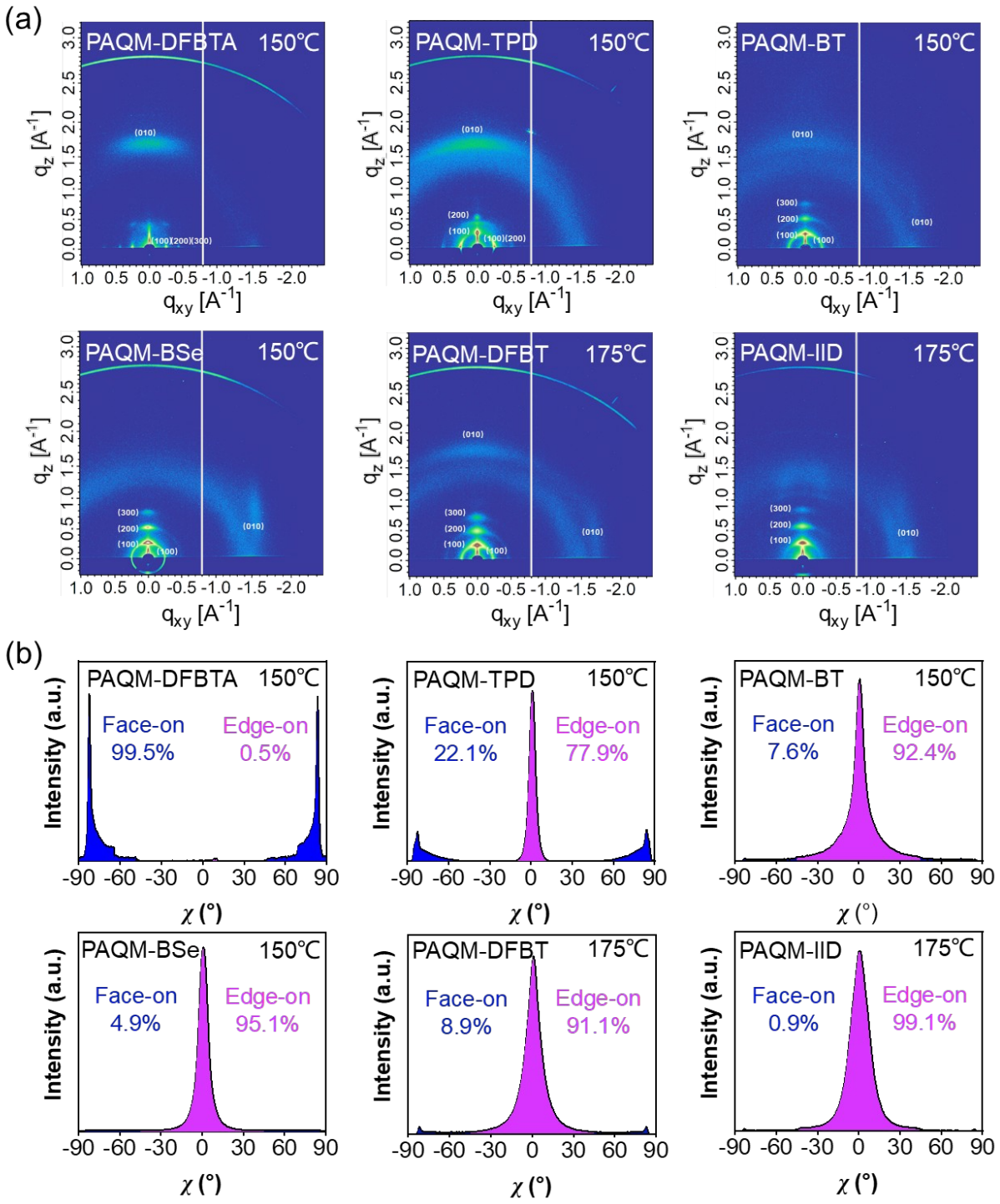

Figure 5. a) GIWAXS patterns of annealed Q-D-A polymer films. b) The pole profiles extracted from the (100) diffraction peaks of annealed Q-D-A polymer films, where the peak areas in the ranges of $0 \leq |\chi| \leq 45°$ and $45 \leq |\chi| \leq 90°$ correspond to edge-on and face-on crystallites, respectively.

peaks in the out-of-plane (OOP) direction and (h00) diffraction peaks (h is up to 3) in the in-plane (IP) direction, indicating a pure face-on orientation. In addition, not only OOP (010)

diffraction and IP (h00) (h decreased to 2) diffraction were maintained in PAQM-TPD, but also OOP (h00) (h=1~2) diffraction showed up, which corresponded to a bimodal orientation with the coexistence of face-on and edge-on lamellas. In the case of PAQM-BT, PAQM-BSe and PAQM-DFBT, OOP (010) diffraction appeared to be largely weakened and the order of IP (h00) diffraction decreased to 1, where the IP (010) diffraction showed up with the order of OOP (h00) diffraction increased to 3, resulting in a predominant edge-on orientation with only a small fraction of face-on orientation. Regarding PAQM-IID, strong OOP (h00) diffraction peaks (h=1~3) together with the absence of OOP (010) and IP (100) diffraction peaks implied a pure edge-on orientation for PAQM-IID with high crystallinity. Pole profiles extracted from the (100) diffraction peaks of annealed Q-D-A polymer films were constructed, from which the ratios of face-on to edge-on were calculated for each polymer by calculating the area ratios of the two regions (χ = 0–45° and 45–90°).[27] As revealed in **Figure 5b**, PAQM-DFBTA show an almost pure face-on orientation with face-on proportion of 99.5%, whereas the PAQM-TPD exhibit a clear bimodal texture (face-on (22.1%) versus edge-on (77.9%)). The face-on/edge-on ratios were 7.6/92.4, 4.9/95.1, and 8.9/91.1 for PAQM-BT, PAQM-BSe and PAQM-DFBT, respectively, indicating the predominately edge-on oriented crystallites in their films. For PAQM-IID, it adopts a nearly pure edge-on orientation, evidenced by an edge-on crystallite proportion of 99.1%. It should be noted that, all the Q-D-A polymers have identical quinoid and donor unit but different acceptor unit, where the acceptor strength follows the order that IID> DFBT> BSe> BT> TPD> DFBTA.[28] Interestingly, the results demonstrate a direct correlation between acceptor strength and crystallite orientation in Q-D-A polymers. The orientation transition from pure face-on in PAQM-DFBTA to bimodal in PAQM-TPD, and to predominant edge-on in PAQM-BT, PAQM-BSe and PAQM-DFBT, and finally to pure edge-on in PAQM-IID suggests that polymers have a stronger tendency to form edge-on lamellas as acceptor strength increase, as illustrated in **Figure 6**. In addition, the relatively small fraction of edge-on crystallites and low crystallinity in PAQM-DFBTA and PAQM-TPD may account for their inferior hole mobilities to other polymers. In the case of PAQM-BSe, PAQM-DFBT and PAQM-IID, we conducted the calculations of the crystalline coherence lengths (CCL), which represented the crystalline size.[29] The CCLs were 370, 282 and 242 Å for PAQM-BSe, PAQM-DFBT and PAQM-IID, respectively. The smaller CCL for PAQM-IID correlates well with its lower mobility than that of PAQM-DFBT. The lack of direct correlation between molecular weight and hole mobility in Q-D-A polymers indicates that, despite the larger CCL of 370 Å for PAQM-BSe, the relatively large effective hole

masses and weak interchain interactions may be responsible for its poor mobility. Furthermore, PAQM-DFBT showed relatively higher crystallinity, larger fraction of edge-on crystallite, stronger interchain interactions and smaller effective hole masses, all contributing to the excellent charge transport mobility. On the other hand, as depicted in Figure S15 (Supporting Information), all Q-D-A polymer films displayed distinctive diffraction peaks without thermal annealing, revealing their intrinsically crystalline nature, which correlated well with their decent effective hole mobilities. Despite the relatively low crystallinity of the as-cast thin-films, PAQM-DFBTA and PAQM-TPD adopted a face-on orientation, while PAQM-BT, PAQM-BSe and PAQM-DFBT showed bimodal textures with the existence of both face-on and edge-on orientations. In addition, a primarily edge-on orientation with a small fraction of face-on orientation was observed in the film of PAQM-IID polymer. The trend of the crystallite orientation changing with varied acceptor strength in as-cast films is similar to that in annealed films, where Q-D-A polymers tend to form edge-on lamellas as the acceptor strength increases. Upon thermal annealing, the crystallinity of all Q-D-A polymer films is significantly enhanced, evidenced by the more pronounced and sharper diffraction peaks, where edge-on is the thermodynamically more preferred orientation except PAQM-DFBTA.

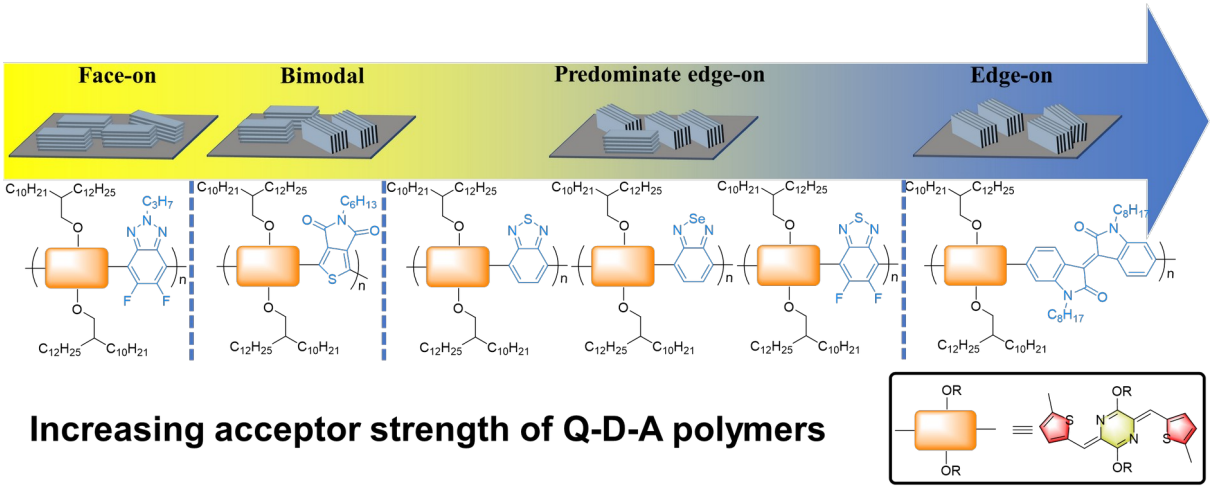

Figure 6. Summary of the dependence of crystallite orientations on the acceptor strength of Q-D-A polymers.

Tapping-mode atomic force microscopic (AFM) characterization of the annealed films was carried out and presented in **Figure 7**. The AFM image of the PAQM-BT film annealed at 150 °C was also included for comparison. All of the films exhibited distinguishable grains, which correlated well with their crystalline features. The root mean square (RMS) roughness

of PAQM-DFBTA and PAQM-TPD were ca. 0.65 nm, respectively, which were rather small and agreed well with their relatively low crystallinity. The other four polymers with relatively high crystallinity displayed larger interconnected domains with RMS values of over 1 nm, which could facilitate charge transport across different crystalline grain boundaries to give higher carrier mobilities.[30] In the case of as-cast films, all the Q-D-A polymers showed rather smooth microstructures with lower RMS values of 0.43–0.67 nm, which correlated well with their lower crystallinity and hole mobilities compared to their annealed films (Figure S16, Supporting Information). The enhanced crystallinity of annealed film could be attributed to the rearrangement of polymer chains during the annealing process.[31]

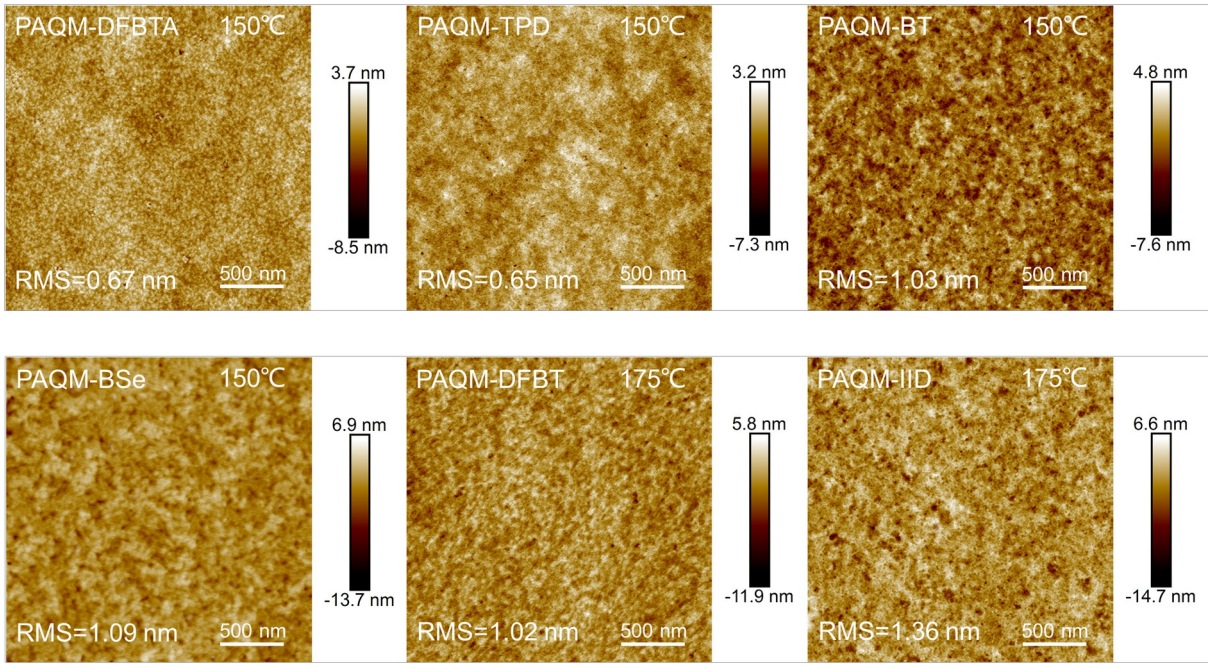

Figure 7. AFM images of annealed Q-D-A polymer films.

2.6. OFET Device Stability

Considering the practical application, operational stability is as essential as environmental stability for OFETs device. As shown in Figure S17 (Supporting Information), all the devices exhibited only slight changes in transfer characteristics after being stored in air at a relative humidity of ca. 80% for over one month, except slight degradation in the case of PAQM-DFBTA. Their decent air stability is crucial for device storage and practical usage. In addition, operational stabilities were also evaluated by applying the continuous cycle testing (9000 cycles, 4000 s, V_G of –80 and 0 V at fixed V_{DS} of –80 V).[16b, 32] As shown in **Figure 8a**, both the on-current and off-current of PAQM-DFBTA were decreased by ~77% and ~65%,

respectively, accompanied by a slightly lowered on/off ratio, indicating the adverse operational stability. Similar degradation behavior was observed in PAQM-TPD, with on-current and off-current decreased by ~37% and ~49%, respectively, which however was much better than PAQM- DFBTA. Despite the fluctuation in off-current, devices based on PAQM-BT and PAQM-BSe showed improved stability with less fall in on-current and off-current. Moreover, PAQM-DFBT

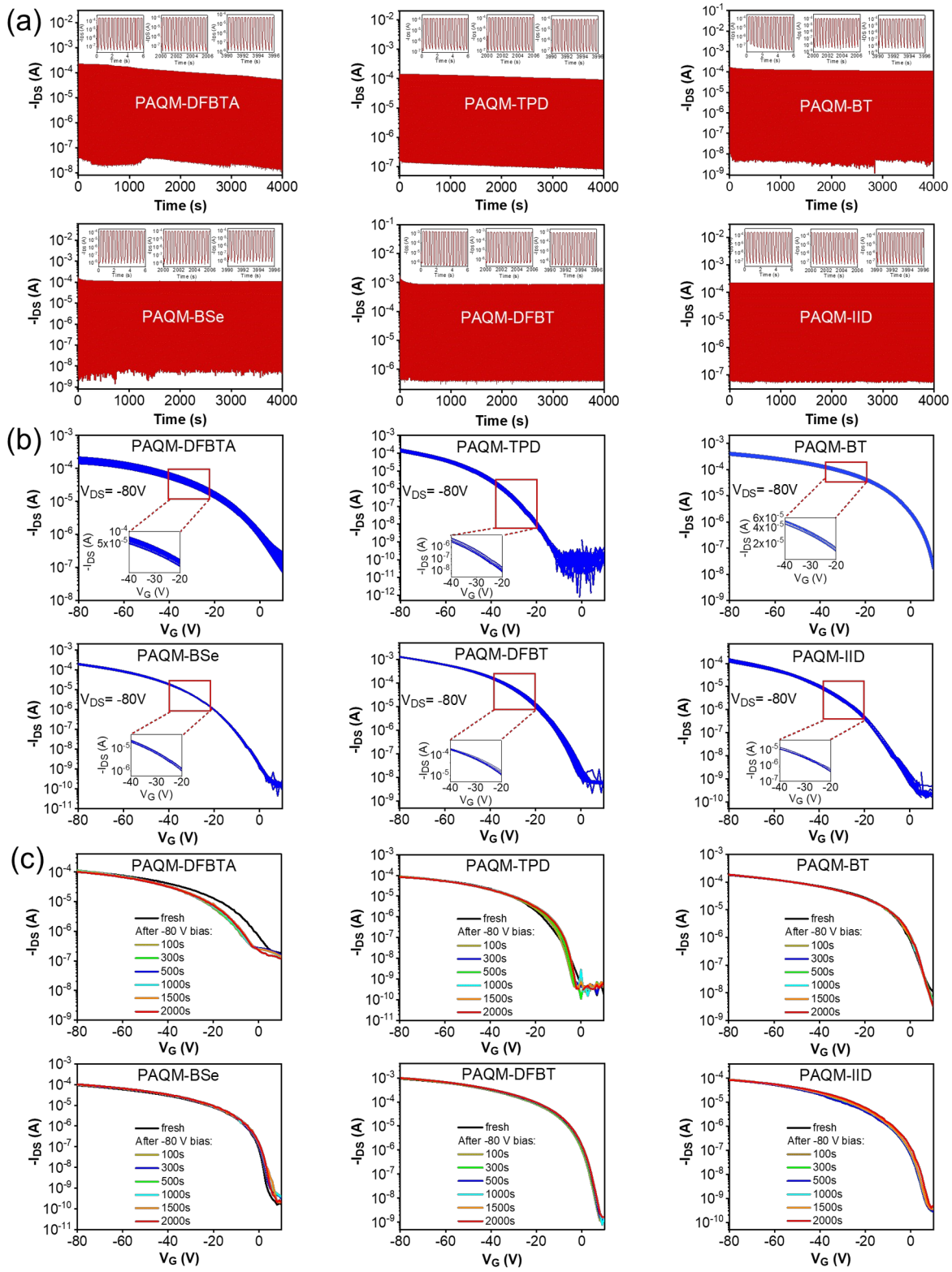

Figure 8. a) On-off cycle tests (9000 cycles) of OFETs based on Q-D-A polymers, which were performed by applying V_G of −80 and 0 V at V_{DS} of −80 V. b) Repeatability of series of transfer characteristics of OFETs based on Q-D-A polymers with 30 cycles at V_{DS} of −80 V.

c) Bias stress stability of OFETs based on Q-D-A polymers with prolonged applied bias voltage of −80 V for up to 2000 s.

displayed regular wavelike curves and slightly eroded on-current, demonstrating much enhanced stability. Finally, greatest operational stability was achieved in PAQM-IID, with perfect wavelike curves and negligible changes in the transfer characteristics. The results revealed the correlation between acceptor strength and operational stability in Q-D-A polymers, where polymers based on stronger acceptor units showed better operational stability. Additionally, transfer curves were measured for 30 cycles to evaluate the repeatability,[32] where similar correlation was also observed (**Figure 8b**). As the acceptor strength increases, better repeatability of the OFETs device is realized. Furthermore, bias stress stability of OFETs based on Q-D-A polymers were investigated under a continuous bias voltage of −80 V for up to 2000 s. As shown in **Figure 8c**, the transfer curves varied little with the exception of PAQM-DFBTA and PAQM-TPD, of which the trend is in excellent agreement with that from cycling test and repeatability evaluation. It has been reported previously that operational stabilities are associated with the crystallinity of the polymer films.[33] OFETs based on Q-D-A polymers with stronger acceptor units are more inclined to deliver decent operational stabilities, presumably due to the higher crystallinities of the polymer films. It should be noted that the molecular weights of Q-D-A polymers in this work were kept relatively low for processability considerations. Optimization of molecular weights of Q-D-A polymers may further facilitate the charge transport and enhance the device stability.

3. Conclusion

In summary, we have conducted a comprehensive study to reveal the potential of the Q-D-A strategy by varying the acceptor strength in Q-D-A conjugated polymers. Five Q-D-A polymers with different electron acceptor units were synthesized and characterized, with particular emphasis on probing backbone geometries, optoelectronic properties, thin film morphologies, charge transport properties and OFET device stabilities. Together with the previously reported polymer PAQM-BT, enforced backbone coplanarity and orders-of-magnitude enhancement of hole transport were achieved by insertion of quinoid unit into the backbone of D-A polymers, confirming the effectiveness of the Q-D-A strategy in manipulating the backbone conformation and boosting the hole mobility of semiconducting polymers. Notably, mobilities of up to 3.35 $cm^2 V^{-1} s^{-1}$ was obtained, which is one of the

highest among the quinoidal-aromatic polymers, highlighting the great potential of Q-D-A strategy in producing high-performing semiconducting polymers. It is further revealed that acceptor unit has little influence on HOMO levels of Q-D-A polymers but more impact on LUMO levels, effective hole masses, film crystallinity, crystallite orientation and device operational stability. Polymers composed of stronger acceptor units have shown a stronger tendency to exhibit efficient intrachain transport, high film crystallinity, edge-on crystallite and good operational stability. The exact nature of this correlation, and whether this is unique to the Q-D-A system, however, remain to be unraveled and encourage future endeavors.[34] In addition, the unipolar *p*-type transport of Q-D-A polymers with rather deep LUMO levels prompt further studies towards exploring the hitherto unobserved electron-transporting properties in such Q-D-A polymers. Nonetheless, the revealed structure-property-device performance relationship is essential to inform the search for high performance, more practical semiconducting polymers based on the underexplored Q-D-A strategy.

Supporting Information

Supporting Information is available from the Wiley Online Library or from the author.

Acknowledgements

H.L., C.L. and Z.Z. contributed equally to this work. This work was supported by Natural Science Special Foundation of Guizhou University (X2019062 and 201905), Nature Science Foundation of Guizhou Provincial Science and Technology Department (QKHJC ZK [2021] general 247), Fundamental Research Key Project of Guizhou Province (20201Z044), Guizhou Science Fund for Excellent Young Scholars (20195665), National Natural Science Foundation of China (22179040), Basic and Applied Basic Research Major Program of Guangdong Province (2019B030302007), Cooperative Program of Taiyuan University of Technology and Guizhou University(202101). Part of the work was performed as a user project at the Molecular Foundry, a national user facility supported by the Office of Science, Office of Basic Energy Sciences, of the U.S. Department of Energy under Contract No. DE-AC02-05CH11231. G.Z. acknowledges the financial support from First-class Physics Promotion Programme (2019) of Guizhou University.

Received: ((will be filled in by the editorial staff))

Revised: ((will be filled in by the editorial staff))

Published online: ((will be filled in by the editorial staff))

References

[1] a) Q. Zhang, T. Jin, X. Ye, D. Geng, W. Chen, W. Hu, *Adv. Funct. Mater.* **2021**, 31, 2106151; b) X. Wu, R. Jia, J. Pan, J. Wang, W. Deng, P. Xiao, X. Zhang, J. Jie, *Adv. Funct. Mater.* **2021**, 31, 2100202; c) D. Liu, J. Mun, G. Chen, N. J. Schuster, W. Wang, Y. Zheng, S. Nikzad, J.-C. Lai, Y. Wu, D. Zhong, Y. Lin, Y. Lei, Y. Chen, S. Gam, J. W. Chung, Y. Yun, J. B. H. Tok, Z. Bao, *J. Am. Chem. Soc.* **2021**, 143, 11679; d) T.-J. Ha, P. Sonar, A. Dodabalapur, *ACS Appl. Mater. Interfaces* **2014**, 6, 3170; e) H. Dong, X. Fu, J. Liu, Z. Wang, W. Hu, *Adv. Mater.* **2013**, 25, 6158; f) A. Facchetti, *Nat. Mater.* **2013**, 12, 598.

[2] a) Z.-F. Yao, Y.-Q. Zheng, J.-H. Dou, Y. Lu, Y.-F. Ding, L. Ding, J.-Y. Wang, J. Pei, *Adv. Mater.* **2021**, 33, 2006794; b) X. Yu, C. Li, C. Gao, X. Zhang, G. Zhang, D. Zhang, *SmartMat.* **2021**, 2, 347; c) K. Feng, H. Guo, H. Sun, X. Guo, *Acc. Chem. Res.* **2021**, 54, 3804; d) R. Zhao, Y. Min, C. Dou, B. Lin, W. Ma, J. Liu, L. Wang, *ACS Appl. Polym. Mater.* **2020**, 2, 19; e) Y. Min, C. Dou, H. Tian, Y. Geng, J. Liu, L. Wang, *Angew. Chem. Int. Ed.* **2018**, 57, 2000; f) P. Sonar, J. Chang, Z. Shi, E. Gann, J. Li, J. Wu, C. R. McNeill, *J. Mater. Chem. C* **2015**, 3, 9299.

[3] a) L. Janasz, M. Borkowski, P. W. M. Blom, T. Marszalek, W. Pisula, *Adv. Funct. Mater.* **2022**, 32, 2105456; b) P. Kafourou, B. Park, J. Luke, L. Tan, J. Panidi, F. Glöcklhofer, J. Kim, T. D. Anthopoulos, J.-S. Kim, K. Lee, S. Kwon, M. Heeney, *Angew. Chem. Int. Ed.* **2021**, 60, 5970.

[4] a) S. Park, S. H. Kim, H. H. Choi, B. Kang, K. Cho, *Adv. Funct. Mater.* **2020**, 30, 1904590; b) P. A. Bobbert, A. Sharma, S. G. J. Mathijssen, M. Kemerink, D. M. de Leeuw, *Adv. Mater.* **2012**, 24, 1146.

[5] a) Y. Xu, C.-W. Ju, B. Li, Q.-S. Ma, Z. Chen, L. Zhang, J. Chen, *ACS Appl. Mater. Interfaces* **2021**, 13, 34033; b) K. Gao, Y. Kan, X. Chen, F. Liu, B. Kan, L. Nian, X. Wan, Y. Chen, X. Peng, T. P. Russell, Y. Cao, A. K.-Y. Jen, *Adv. Mater.* **2020**, 32, 1906129; c) L. Nian, Y. Kan, K. Gao, M. Zhang, N. Li, G. Zhou, S. B. Jo, X. Shi, F. Lin, Q. Rong, F. Liu, G. Zhou, A. K. Y. Jen, *Joule* **2020**, 4, 2223; d) H. Jiang, F. Pan, L. Zhang, X. Zhou, Z. Wang, Y. Nian, C. Liu, W. Tang, Q. Ma, Z. Ni, M. Chen, W. Ma, Y. Cao, J. Chen, *ACS Appl. Mater. Interfaces* **2019**, 11, 29094; e) L. Ying, F. Huang, G. C. Bazan, *Nat. Commun.* **2017**, 8, 14047; f) T.-J. Ha, P. Sonar, A. Dodabalapur, *Appl. Phys. Lett.* **2011**, 98, 253305.

[6] a) H. Jiang, G. Qin, L. Zhang, F. Pan, Z. Wu, Q. Wang, G. Wen, W. Zhang, Y. Cao, J. Chen, *J. Mater. Chem. C* **2021**, 9, 249; b) J. Chen, J. Yang, Y. Guo, Y. Liu, *Adv. Mater.* **2021**, 33, 2104325.

[7] a) L. Luo, W. Huang, C. Yang, J. Zhang, Q. Zhang, *Front. Phys.* **2021**, 16, 33500; b) M. Kim, S. U. Ryu, S. A. Park, K. Choi, T. Kim, D. Chung, T. Park, *Adv. Funct. Mater.* **2020**, 30, 1904545; c) J. Miao, H. Li, T. Wang, Y. Han, J. Liu, L. Wang, *J. Mater. Chem. A* **2020**, 8, 20998; d) X. Liu, L. Nian, K. Gao, L. Zhang, L. Qing, Z. Wang, L. Ying, Z. Xie, Y. Ma, Y. Cao, F. Liu, J. Chen, *J. Mater. Chem. A* **2017**, 5, 17619; e) H. Sirringhaus, *Adv. Mater.* **2014**, 26, 1319; f) T.-J. Ha, P. Sonar, A. Dodabalapur, *Phys. Chem. Chem. Phys.* **2013**, 15, 9735.

[8] a) Y. Wang, T. Hasegawa, H. Matsumoto, T. Michinobu, *J. Am. Chem. Soc.* **2019**, 141, 3566; b) Y. Kim, H. Hwang, N.-K. Kim, K. Hwang, J.-J. Park, G.-I. Shin, D.-Y. Kim, *Adv. Mater.* **2018**, 30, 1706557.

[9] a) J. Kim, A. R. Han, J. Hong, G. Kim, J. Lee, T. J. Shin, J. H. Oh, C. Yang, *Chem. Mater.* **2014**, 26, 4933; b) H. Chen, Y. Guo, G. Yu, Y. Zhao, J. Zhang, D. Gao, H. Liu, Y. Liu, *Adv. Mater.* **2012**, 24, 4618.

[10] a) J. Yang, Q. Liu, M. Hu, S. Ding, J. Liu, Y. Wang, D. Liu, H. Gao, W. Hu, H. Dong, *Sci. China: Chem.* **2021**, 64, 1410; b) X. Guo, Q. Liao, E. F. Manley, Z. Wu, Y. Wang, W. Wang, T. Yang, Y.-E. Shin, X. Cheng, Y. Liang, L. X. Chen, K.-J. Baeg, T. J. Marks, X. Guo, *Chem. Mater.* **2016**, 28, 2449; c) T. Lei, X. Xia, J.-Y. Wang, C.-J. Liu, J. Pei, *J. Am. Chem. Soc.* **2014**, 136, 2135.

[11] a) Y. Wang, H. Guo, A. Harbuzaru, M. A. Uddin, I. Arrechea-Marcos, S. Ling, J. Yu, Y. Tang, H. Sun, J. T. López Navarrete, R. P. Ortiz, H. Y. Woo, X. Guo, *J. Am. Chem. Soc.* **2018**, 140, 6095; b) G. K. Dutta, A. R. Han, J. Lee, Y. Kim, J. H. Oh, C. Yang, *Adv. Funct. Mater.* **2013**, 23, 5317.

[12] a) M. Yang, T. Du, X. Zhao, X. Huang, L. Pan, S. Pang, H. Tang, Z. Peng, L. Ye, Y. Deng, S. Mingliang, C. Duan, H. Fei, C. Yong, *Sci. China: Chem.* **2021**, 64, 1219; b) X. Ji, L. Fang, *Polym. Chem.* **2021**, 12, 1347; c) L. Pan, T. Zhan, J. Oh, Y. Zhang, H. Tang, M. Yang, M. Li, C. Yang, X. Liu, P. Cai, C. Duan, F. Huang, Y. Cao, *Chem. Eur. J.* **2021**, 27, 13527; d) J. Huang, G. Yu, *Mater. Chem. Front.* **2021**, 5, 76; e) T. Du, R. Gao, Y. Deng, C. Wang, Q. Zhou, Y. Geng, *Angew. Chem. Int. Ed.* **2020**, 59, 221; f) J. Huang, S. Lu, P.-A. Chen, K. Wang, Y. Hu, Y. Liang, M. Wang, E. Reichmanis, *Macromolecules* **2019**, 52, 4749; g) C. Zhang, X. Zhu, *Acc. Chem. Res.* **2017**, 50, 1342.

[13] a) X. Liu, B. He, A. Garzon-Ruiz, A. Navarro, T. L. Chen, M. A. Kolaczkowski, S. Feng, L. Zhang, C. A. Anderson, J. Chen, Y. Liu, *Adv. Funct. Mater.* **2018**, 28, 201801874; b) X. Liu, B. He, C. L. Anderson, J. Kang, T. Chen, J. Chen, S. Feng, L. Zhang, M. A. Kolaczkowski, S. J. Teat, M. A. Brady, C. Zhu, L.-W. Wang, J. Chen, Y. Liu, *J. Am. Chem. Soc.* **2017**, 139, 8355.

[14] a) C. L. Anderson, H. Li, C. G. Jones, S. J. Teat, N. S. Settineri, E. A. Dailing, J. Liang, H. Mao, C. Yang, L. M. Klivansky, X. Li, J. A. Reimer, H. M. Nelson, Y. Liu, *Nat. Commun.* **2021**, 12, 6818; b) L. Wang, X. Liu, X. Shi, C. L. Anderson, L. M. Klivansky, Y. Liu, Y. Wu, J. Chen, J. Yao, H. Fu, *J. Am. Chem. Soc.* **2020**, 142, 17892; c) C. L. Anderson, N. Dai, S. J. Teat, B. He, S. Wang, Y. Liu, *Angew. Chem. Int. Ed.* **2019**, 58, 17978.

[15] C. Liu, X. Liu, G. Zheng, X. Gong, C. Yang, H. Liu, L. Zhang, C. L. Anderson, B. He, L. Xie, R. Zheng, H. Liang, Q. Zhou, Z. Zhang, J. Chen, Y. Liu, *J. Mater. Chem. A* **2021**, 9, 23497.

[16] a) X. Liu, P. Cai, Z. Chen, L. Zhang, X. Zhang, J. Sun, H. Wang, J. Chen, J. Peng, H. Chen, Y. Cao, *Polymer* **2014**, 55, 1707; b) X. Guo, R. P. Ortiz, Y. Zheng, M.-G. Kim, S. Zhang, Y. Hu, G. Lu, A. Facchetti, T. J. Marks, *J. Am. Chem. Soc.* **2011**, 133, 13685; c) P. Sonar, E. L. Williams, S. P. Singh, A. Dodabalapur, *J. Mater. Chem.* **2011**, 21, 10532; d) A. Bedi, S. P. Senanayak, S. Das, K. S. Narayan, S. S. Zade, *Polym. Chem.* **2012**, 3, 1453; e) P. Cai, Z. Chen, L. Zhang, J. Chen, Y. Cao, *J. Mater. Chem. C* **2017**, 5, 2786; f) T. Lei, Y. Cao, X. Zhou, Y. Peng, J. Bian, J. Pei, *Chem. Mater.* **2012**, 24, 1762.

[17] Z.-Y. Wang, L. Di Virgilio, Z.-F. Yao, Z.-D. Yu, X.-Y. Wang, Y.-Y. Zhou, Q.-Y. Li, Y. Lu, L. Zou, H. I. Wang, X.-Y. Wang, J.-Y. Wang, J. Pei, *Angew. Chem. Int. Ed.* **2021**, 60, 20483.
[18] C. P. Yau, Z. Fei, R. S. Ashraf, M. Shahid, S. E. Watkins, P. Pattanasattayavong, T. D. Anthopoulos, V. G. Gregoriou, C. L. Chochos, M. Heeney, *Adv. Funct. Mater.* **2014**, 24, 678.
[19] K. Shi, W. Zhang, D. Gao, S. Zhang, Z. Lin, Y. Zou, L. Wang, G. Yu, *Adv. Mater.* **2018**, 30, 1705286.
[20] C. Zhu, L. Fang, *Macromol. Rapid Commun.* **2018**, 39, 1700241.
[21] a) C. Cheng, H. Geng, Y. Yi, Z. Shuai, *J. Mater. Chem. C* **2017**, 5, 3247; b) J. Yang, Z. Zhao, H. Geng, C. Cheng, J. Chen, Y. Sun, L. Shi, Y. Yi, Z. Shuai, Y. Guo, S. Wang, Y. Liu, *Adv. Mater.* **2017**, 29, 201702115.
[22] Y. Xu, H. Sun, A. Liu, H. Zhu, B. Li, T. Minari, F. Balestra, G. Ghibaudo, Y.-Y. Noh, *Adv. Funct. Mater.* **2018**, 28, 1803907.
[23] a) H. H. Choi, K. Cho, C. D. Frisbie, H. Sirringhaus, V. Podzorov, *Nat. Mater.* **2018**, 17, 2; b) Y. Xu, Y. Li, S. Li, F. Balestra, G. Ghibaudo, W. Li, Y.-F. Lin, H. Sun, J. Wan, X. Wang, Y. Guo, Y. Shi, Y.-Y. Noh, *Adv. Funct. Mater.* **2020**, 30, 1904508.
[24] a) W. Xu, S.-W. Rhee, *J. Mater. Chem.* **2009**, 19, 5250; b) F. Yang, L. Sun, J. Han, B. Li, X. Yu, X. Zhang, X. Ren, W. Hu, *ACS Appl. Mater. Interfaces* **2018**, 10, 25871.
[25] G. Murtaza, I. Ahmad, H. Chen, J. Wu, *Synth. Met.* **2014**, 194, 146.
[26] a) W. Wu, Y. Liu, D. Zhu, *Chem. Soc. Rev.* **2010**, 39, 1489; b) M. Kano, T. Minari, K. Tsukagoshi, *Appl. Phys. Lett.* **2009**, 94, 143304.
[27] a) G. Kim, S.-J. Kang, G. K. Dutta, Y.-K. Han, T. J. Shin, Y.-Y. Noh, C. Yang, *J. Am. Chem. Soc.* **2014**, 136, 9477; b) Z. Wang, Z. Liu, L. Ning, M. Xiao, Y. Yi, Z. Cai, A. Sadhanala, G. Zhang, W. Chen, H. Sirringhaus, D. Zhang, *Chem. Mater.* **2018**, 30, 3090.
[28] M. E. Köse, *J. Phys. Chem. A* **2012**, 116, 12503.
[29] J. Lee, A. R. Han, H. Yu, T. J. Shin, C. Yang, J. H. Oh, *J. Am. Chem. Soc.* **2013**, 135, 9540.
[30] Q. Liu, Y. Wang, A. Kohara, H. Matsumoto, S. Manzhos, K. Feron, S. E. Bottle, J. Bell, T. Michinobu, P. Sonar, *Adv. Funct. Mater.* **2020**, 30, 1907452.
[31] Y. Ding, Y. Zhu, X. Wang, Y. Wang, S. Zhang, G. Zhang, X. Gu, L. Qiu, *Chem. Mater.* **2022**, 34, 2696.
[32] S. Wang, Z. Wang, Y. Huang, Y. Hu, L. Yuan, S. Guo, L. Zheng, M. Chen, C. Yang, Y. Zheng, J. Qi, L. Yu, H. Li, W. Wang, D. Ji, X. Chen, J. Li, L. Li, W. Hu, *ACS Appl. Mater. Interfaces* **2021**, 13, 17852.
[33] W. H. Lee, H. H. Choi, D. H. Kim, K. Cho, *Adv. Mater.* **2014**, 26, 1660.
[34] a) M. S. Chen, O. P. Lee, J. R. Niskala, A. T. Yiu, C. J. Tassone, K. Schmidt, P. M. Beaujuge, S. S. Onishi, M. F. Toney, A. Zettl, J. M. J. Fréchet, *J. Am. Chem. Soc.* **2013**, 135, 19229; b) M. S. Chen, J. R. Niskala, D. A. Unruh, C. K. Chu, O. P. Lee, J. M. J. Fréchet, *Chem. Mater.* **2013**, 25, 4088.

The potential of underexplored quinoid-donor-acceptor strategy for developing practical semiconducting polymers and the role of electron acceptors are comprehensively investigated, leading to high-performance transistors with higher mobilities and robust storage and operational stabilities. Polymers with stronger acceptor units tend to deliver edge-on lamellas, high film crystallinity, small effective hole masses and decent operational stability.

Huanhuan Liang, Cheng Liu, Zesheng Zhang, Xuncheng Liu,* Quanfeng Zhou, Guohui Zheng, Xiu Gong, Lan Xie, Chen Yang, Lianjie Zhang, Bo He, Junwu Chen* and Yi Liu*

Unravelling the Role of Electron Acceptors for the Universal Enhancement of Charge Transport in Quinoid-Donor-Acceptor Polymers for High-Performance Transistors